PACS numbers: 42.60.Jf; 42.79.–e
DOI: 10.1070/QE2006v036n10ABEH013258

Compensation for thermally induced aberrations in optical elements by means of additional heating by CO_2 laser radiation

A.A. Soloviev, I.E. Kozhevatov, O.V. Palashov, E.A. Khazanov

***Abstract*. A method is proposed for compensating thermally induced phase distortions of laser radiation in absorbing optical elements. The method is based on supplementary heating of the peripheral region of the distorting element by the radiation from an auxiliary laser. A programme code has been developed for calculating the optimal parameters of supplementary radiation to minimise phase distortions. This code is based on the numerical solution of the thermal conductivity and static elasticity equations for a nonuniformly heated element of cylindrical symmetry. Experiments reveal a high efficiency of the method for compensating distortions resulting from absorption of radiation with a Gaussian intensity profile.**

Keywords: *thermal phase distortions, aberration, phase-modulated interferometric measurements, thermally induced deformation, laser beam scanning.*

1. Introduction

The advancement of laser engineering and applied technologies has led to the development of highly sophisticated lasers which are being used in new projects that require high-power high-intensity laser beams and strong fields. The laser beam quality must remain extremely high in this case. A high mean power of laser radiation results in a considerable heat release in optical elements and calls for special attention to the problems of thermal effects leading to a distortion of the radiation phase front. Hence it is important to develop various methods of reducing such distortions. The most popular techniques are based on the use of a removable compensating lens or a tunable telescope [1 – 4], which allows elimination of the quadratic distortion component. More complicated aberrations are compensated by using adaptive optical techniques such as phase conjugation [5], adaptive mirrors [6, 7] and elements capable of modulating the transmitted radiation phase [8], as well as auxiliary optical elements in which a compensating thermal lens is formed due to absorption [9 – 13].

Our paper is devoted to the so-called active thermal compensation based on the heating of an optical element, which reduces the radiation phase distortions [14, 15].

Additional heating can be performed either due to heat conduction (thermal contact) or by radiation (contactless). Radiative heating rules out mechanical damage of optical elements during adjustment and compensation stages. The use of incoherent radiation for thermal compensation is hampered due to the problems associated with the control of compensating heating profile. In this research, a laser beam is used for additional heating, while the required ring-shaped intensity distribution profile is attained by displacing the laser beam along a circular trajectory at the optical element aperture. An analogous but more complicated approach was proposed in [14] where compensation of thermal distortions was not demonstrated experimentally. Note that our approach cannot completely eliminate the wavefront distortions (e.g., to produce a plane wavefront) in the general case, but can considerably suppress aberrations in the stationary as well as nonstationary case.

Note that heat release in the sample always leads to an increase in the mean temperature of the optical element, which is undesirable in many cases (e.g., due to an increase in the thermal noise). Hence, we used surface heating which leads to the same compensation in the steady state as in the case of bulk heating, and at the same time reduces the released thermal power (see details below). Surface heating was performed by 10.6-μm CO_2 laser radiation which is absorbed strongly in a number of optical materials like glass and silica.

In this work, we compensated for steady phase distortions of radiation passing through the sample, while the distorting and compensating heating were performed at the sample surface. This case is interesting, for example, for the Laser Interferometer Gravitational Wave Observatory (LIGO) detector [16] in which radiation passes through a number of optical elements subjected to surface heating. We chose the decrease in the radiation power fraction in the initial mode as the quantitative criterion of aberration. In our case, this is the TEM_{00} mode of free space (Gaussian beam).

We present below the results of numerical simulation of the thermal conductivity and elasticity equations. In particular, we determine the values of the compensating radiation parameters. We also describe the experimental setup and discuss the results of measurements.

A.A. Soloviev, I.E. Kozhevatov, O.V. Palashov, E.A. Khazanov Institute of Applied Physics, Russian Academy of Sciences, ul. Ul'yanova 46, Nizhnii Novgorod, 603950 Russia; e-mail: so-lo@appl.sci-nnov.ru

Received 19 May 2006
Kvantovaya Elektronika **36** (10) 939 – 945 (2006)
Translated by Ram Wadhwa

2. Numerical simulation of the compensation of thermal distortions

The aim of the numerical simulation was to calculate the additional heating parameters corresponding to minimum phase distortions. Compensation of thermal distortions requires cylindrically symmetric compensating heating which creates, in the absence of other heat sources, a temperature distribution with a minimum at the centre of symmetry. Such a situation can arise for a circular distribution of the additional heat sources, and surface heating is preferable to bulk heating for lowering the undesirable increase in the mean temperature. This is due to the fact that heat removal from the end faces is larger (than from the lateral surface) during surface heating, and hence a lower power is required to provide a steady temperature distribution with a minimum at the symmetry axis.

We considered the following problem. An optically transparent cylindrical sample (which introduces only phase distortions in the transmitted radiation) of diameter d and length l is heated nonuniformly from its plane end face. Conditions of convective heat exchange are fulfilled at the entire surface of the sample. The heating profile is a superposition of the heating profiles generated by two sources with axially symmetric intensity distribution functions. The first (heating) source is specified by the intensity distribution I_1:

$$I_1(r, w_0) = \frac{P_0}{w_0^2\pi}\exp\left(-\frac{r^2}{w_0^2}\right), \tag{1}$$

where r is the radial coordinate; w_0 is the beam radius; and P_0 is the beam power. The intensity I_2 of the second (compensating) source is described by the expression

$$I_2(r, R, W, P) = \frac{P}{2W^2\pi^2} \times \int_0^{2\pi} \exp\left[\frac{-(r^2 - 2Rr\cos\varphi + R^2)}{W^2}\right]\mathrm{d}\varphi, \tag{2}$$

which corresponds to time-averaged distribution of the energy absorbed during surface heating by a Gaussian beam of power P and radius W, rotating over a circle of radius R. It is assumed that the period of rotation of the beam is much smaller than the characteristic time $\rho c_p W^2/\kappa$ of temperature stabilisation, where ρ, c_p and κ are the density, specific heat and thermal conductivity of the medium, respectively [14]. In this approximation, the problem becomes cylindrically symmetric.

To estimate the phase distortions qualitatively, we introduce the parameter γ characterising power losses in the Gaussian (TEM_{00}) mode due to the energy transfer to higher-order modes:

$$\gamma = 1 - \frac{\left|\int E_0 E^* \mathrm{d}s\right|^2}{\int |E_0|^2 \mathrm{d}s \int |E|^2 \mathrm{d}s},$$

where E_0 and E are the complex amplitudes of the undistorted and distorted fields, respectively. For a beam with an intensity distribution of the type (1), consideration of axial symmetry leads to the following expression:

$$\gamma = 1 - \frac{4}{w_0^4}\left|\int \exp(-r^2/w_0^2)\exp[-\mathrm{i}\Delta\psi(r)]r\mathrm{d}r\right|^2, \tag{3}$$

where $\Delta\psi(r)$ is the phase introduced by the aberrational element. Thus, for a given heating source (1), the variation in the compensating radiation parameters W, R and P in (2) can lead to an increase or a decrease in the value of γ, which can be calculated by using the expression for the thermal phase shift [17]

$$\Delta\psi_p(r) = k\int_0^l \left[-\frac{1}{2}n_0^3\pi_{ppkl}\sigma_{kl} + \frac{\beta T(r,z)}{n_0^3} + (n_0 - 1)\varepsilon_{zz}\right]\mathrm{d}z, \tag{4}$$

where $T(r, z)$ is the sample temperature; n_0 is the unperturbed refractive index of the medium at room temperature; $\beta = \mathrm{d}n/\mathrm{d}T$; π_{ijkl}, σ_{kl} and ε_{ik} are respectively the tensors of photoelastic coefficient, elastic stress and strain; and k is the wave number in vacuum. Integration in (4) is carried out along the spatial axis z coinciding with the propagation direction of radiation. The subscript $p = 1, 2$ corresponds to two radiation polarisations. Because thermally induced birefringence is usually much smaller than the phase distortions ($\Delta\psi_1 - \Delta\psi_2 \ll \Delta\psi_1, \Delta\psi_2$), we shall substitute the mean phase shift $\Delta\psi = (\Delta\psi_1 + \Delta\psi_2)/2$ in (3). One can see from (4) that in order to determine $\Delta\psi$ at each point of the aperture, we must know the temperature T as well as the tensors ε_{ik} and σ_{kl}, which are connected through the linear equation

$$\sigma_{ik} = (-\alpha\Delta T\delta_{ik} + \varepsilon_{ll}\delta_{ik})\left(\lambda + \frac{2}{3}\mu\right) + 2\mu\left(\varepsilon_{ik} - \frac{1}{3}\delta_{ik}\varepsilon_{ll}\right),$$

in which the summation is performed over the dummy index. Here, λ and μ are the Lámé coefficients and $\alpha = L^{-1}(\mathrm{d}L/\mathrm{d}T)$ is the coefficient of linear thermal expansion.

In the case of cylindrical symmetry ($\mathrm{d}/\mathrm{d}\varphi = 0$), the time-dependent temperature distribution is determined from the thermal conductivity equation [18]

$$c_p\rho\frac{\partial T(r,z,t)}{\partial t} = \kappa\nabla^2 T(r,z,t) + q(r,z,t), \tag{5}$$

where q is the volume heat release density. For convective heat exchange, the boundary conditions at the end faces ($z = 0$ and $z = l$) of the cylinder have the form

$$\pm\kappa\frac{\partial T(r,z,t)}{\partial z} = -hT(r,z,t) + q_\mathrm{s}, \tag{6}$$

where h is the convective heat exchange factor and q_s is the surface density of external heat sources. The plus and minus signs on the left-hand side of the above equation correspond to $z = l$ and $z = 0$, respectively. The boundary conditions for the generatrix ($r = d/2$) can be written similarly:

$$\kappa\frac{\partial T(r,z,t)}{\partial r} = -hT(r,z,t) + q_\mathrm{s}. \tag{7}$$

The characteristic absorption length of CO_2 laser radiation in silica is ~ 30 μm, which is much smaller than the typical sample size, and hence we shall assume

that all heat sources are surface sources, i.e., $q_s = I_1 + I_2$ and $q = 0$.

During numerical simulation, differential equation (5) with boundary conditions (6) and (7) was approximated by a system of linear equations connecting the temperatures at the nodes of a two-dimensional equidistant square mesh. The obtained system of equations is solved exactly by matrix sweep method [19]. As a result, the transient temperature field of a sample is obtained for arbitrary heat sources whose distribution is independent of the angular coordinate.

This temperature distribution determines the right-hand side of the static elasticity equation for calculating the deformation vector $\boldsymbol{U}$ for a nonuniformly heated elastic solid [20]:

$$\mu\Delta\boldsymbol{U} + (\lambda+\mu)\nabla(\nabla\boldsymbol{U}) = \alpha\left(\lambda + \frac{2}{3}\mu\right)\nabla T. \tag{8}$$

This equation is solved under boundary conditions corresponding to the absence of normal and cleavage stresses at the sample surface:

$$\sigma_{zz} = \sigma_{rz} = \sigma_{\varphi z} = 0 \ \text{ for } z = 0 \text{ and } z = l,$$
$$\sigma_{rr} = \sigma_{zr} = \sigma_{\varphi r} = 0 \ \text{ for } r = d/2. \tag{9}$$

Note that the stress tensor components $\sigma_{\varphi z}$ and $\sigma_{\varphi r}$ are equal to zero at any point of the sample because of degeneracy in coordinate φ.

Equation (8) with boundary conditions (9) was also approximated on the mesh defined by a system of linear difference equations during the solution of Eqn (5). In turn, this system of equations was solved by Seidel's iterative technique [21]. As a result, the deformation vector field $\boldsymbol{U}$ in the sample was obtained, from which the strain tensor ε_{ik} was determined:

$$\varepsilon_{ik} = \frac{1}{2}\left(\frac{\partial U_i}{\partial r_k} + \frac{\partial U_k}{\partial r_i}\right).$$

Thus, all the terms in Eqn (4) were determined and power losses γ were calculated from (3).

The main purpose of our calculations was to find the global minimum $\gamma_{\min}$ of power losses in the three-dimensional space of parameters W, R and P:

$$\gamma_{\min} = \gamma(W_{\text{opt}}, R_{\text{opt}}, P_{\text{opt}}),$$

where W_{opt}, R_{opt} and P_{opt} are the optimal parameters of compensating radiation for the given distortions. Note that in the general case, an additional heating source (2) cannot provide total compensation of thermal aberrations ($\gamma_{\min} = 0$), and the value of $\gamma_{\min}$ depends on the parameters of the heating beam and the optical element used. The value of $\gamma_{\min}$ is obtained by iterations. Curve (*1*) in Fig. 1 shows the theoretical wavefront distortions caused by a Gaussian beam of radius w_0 and power P_0 in the case of total absorption of radiation at the surface. The introduction of compensating radiation with an intensity of type (2) and optimal parameters W_{opt}, R_{opt} and P_{opt} smoothes out these distortions to a considerable extent [curve (*2*)].

Numerical simulations revealed a high efficiency of the method and form the basis of the experiments.

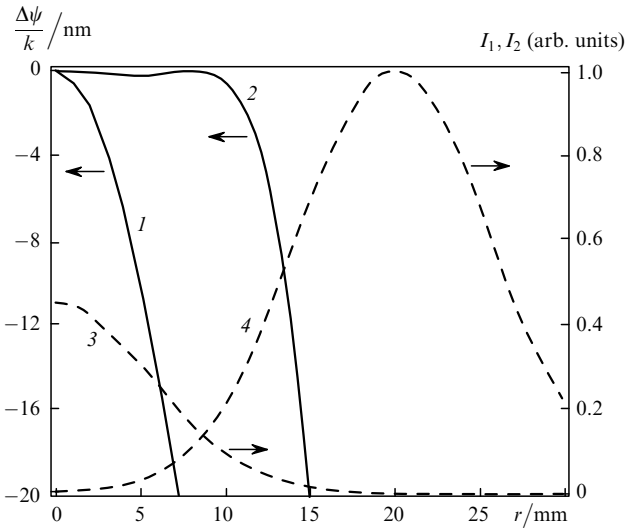

Figure 1. Results of numerical simulation of thermal distortions $\Delta\psi/k$ of the wavefront without [curve (*1*)] and with [curve (*2*)] compensating radiation, as well as spatial distribution of the intensity of heating [I_1, curve (*3*)] and compensating [I_2, curve (*4*)] radiation.

3. Experimental investigations of aberration compensation

Experiments were performed using a setup whose scheme is shown in Fig. 2. The active compensation of thermal phase distortions was simulated by using radiation from 10.6-μm CO_2 laser (*1*), which was split by NaCl wedge (*2*) into three beams. The first beam passed through the wedge and served as the source of compensating radiation, while the second beam, reflected from the rear face of the wedge, served as the heating radiation source. The third beam, reflected from the front face of the wedge, was coupled out from the setup to absorber (*3*). Consider in detail the formation of heating radiation and the radiation compensating phase distortions.

The optical beam reflected from wedge (*2*) entered the unit where heating radiation was produced. Plane mirrors (*4*) and (*5*) were rigidly fixed, while spherical mirror (*6*) (with a radius of curvature $R_0 = 30$ cm) could be displaced continuously in the direction indicated by the arrow, thus allowing for a variation of the heating beam radius at optical sample (*7*). The sample was a 25-mm-thick fused silica cylinder of diameter 100 mm.

After passing through wedge (2), the CO_2 laser beam entered the unit of compensating radiation formation. Spherical mirror (*8*) (with a radius of curvature $R_0 =$ 30 cm) could be displaced continuously to vary the compensating beam radius W. Plane mirror (*9*) was mounted on a specially developed device allowing rotation of the mirror with a frequency of up to 30 Hz around an axis that did not coincide with the normal to the mirror surface. As a result, the required distribution (2) of the average intensity of compensating radiation was produced at the end face of sample (*7*) in the form of a ring with parameters W, R and P. The intensity of both beams was varied with the help of disc choppers (*18*) and (*19*). To avoid the stroboscopic effect, the beam chopping frequency in chopper (*19*) must not be a multiple of the rotational frequency of mirror (*9*). The compensating beam was directed to the sample in such a way that the centre of the ring coincided with the

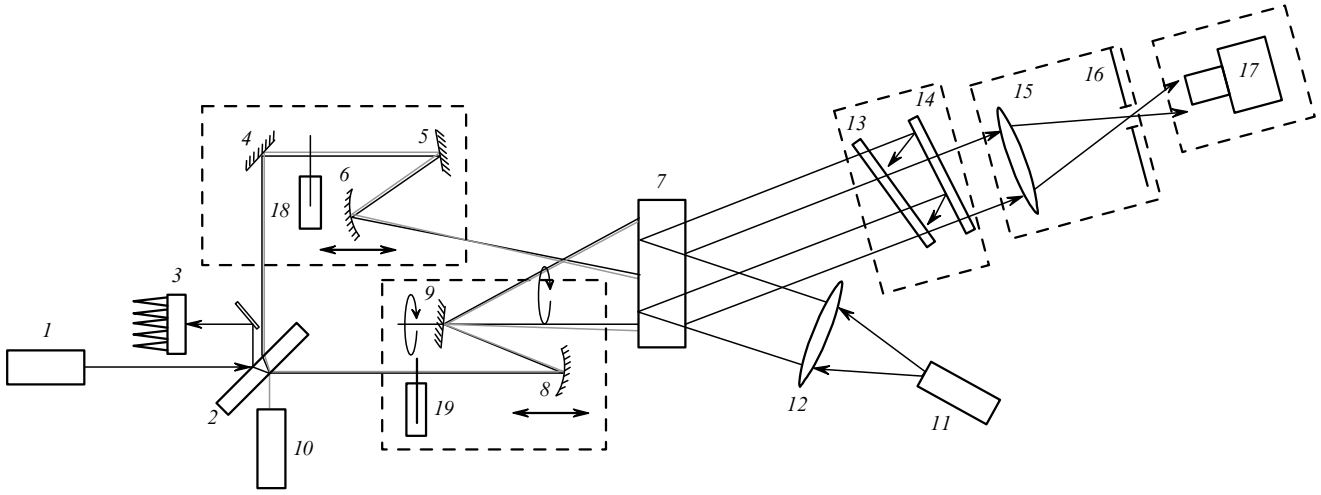

Figure 2. Principal scheme of the experimental setup: (*1*) CO_2 laser; (*2*) NaCl wedge; (*3*) absorber; (*4*, *5*, *9*) plane highly reflecting mirrors; (*6*, *8*) spherical highly reflecting mirrors; (*7*) fused silica sample; (*10*) He–Ne adjustment laser; (*11*) He–Ne stabilisation laser; (*12*) collimating objective; (*13*, *14*) semitransparent mirrors; (*15*) lens; (*16*) diaphragm; (*17*) CCD camera; (*18*, *19*) disc choppers.

symmetry axis, i.e., with the centre of the heating beam. For the convenience of tuning, the CO_2 laser beam was made to coincide with the beam of adjusting He–Ne laser (*10*) at wedge (*2*).

Thermal distortions of the optical thickness of the sample were measured with a reflection interferometer [22]. Radiation from He–Ne laser (*11*) (see Fig. 2), stabilised in power and wavelength, was collimated by objective (*12*) and incident on sample (*7*). The beams reflected from the front and rear faces of the sample were spatially superposed in a conjugation unit consisting of two plane mirrors (*13*) and (*14*). 'Stray' beams generated in the conjugation unit were blocked by an angular filter consisting of lens (*15*) and diaphragm (*16*) located at its focus. The interference pattern formed by two beams from laser (*11*) reflected by sample (*7*) was observed with CCD camera (*17*). The distance between the mirrors in the conjugation unit was modulated mechanically during measurements, thereby changing the interference pattern recorded with the CCD camera. An analysis of such a modulated pattern allows an improvement in the measuring accuracy compared to other interference techniques [23]. Distortions of the optical thickness of the sample were measured with an accuracy of up to $\lambda/1000$ (~ 0.6 nm) [24].

Two measurements are required to obtain the distribution of thermal aberrations in the sample. The optical thickness profile was first measured for the 'cold' sample (without thermal aberrations) and then for the heated sample which already contained thermal distortions. Thermal aberrations were determined as the difference between the results of these two measurements, which could be separated in time by fractions of a second for measurements of transient processes, and by tens of minutes when distortions were caused by steady heating.

For fused silica, the coefficient α is about 20 times smaller than β, which leads to two important consequences. First, thermal distortions of the optical thickness of a fused silica sample (i.e., the distortions measured by the interferometer) do not differ significantly from phase distortions of the test radiation passing through the sample (see [24] for details). Second, the phase profile repeats the temperature profile averaged over the length with a high degree of accuracy. Hence the profile of heat release from the end face of the sample coincides with the phase distortions of the transmitted radiation in the first instants after the onset of heating. Figures 3 and 4 show typical aberration distributions measured with an interferometer within 0.5 s after the CO_2 laser switching. In fact, these distributions correspond

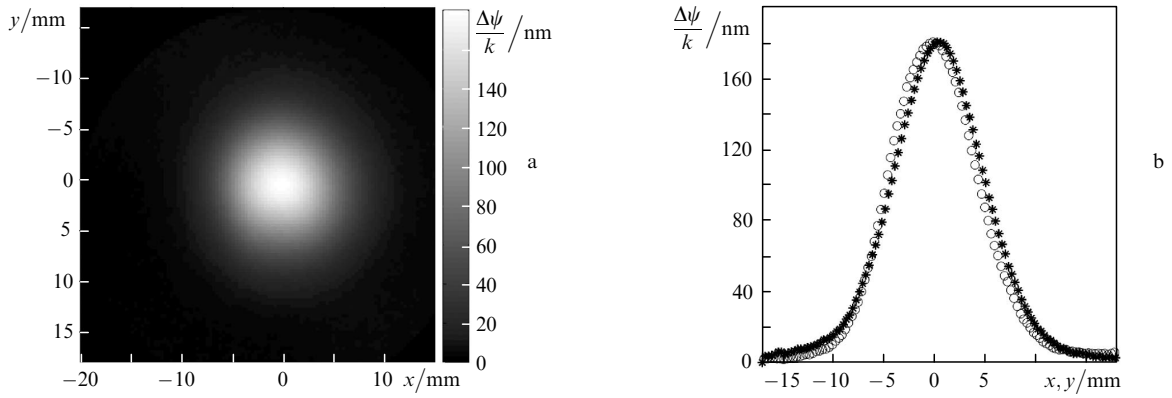

Figure 3. (a) Two-dimensional profile and (b) horizontal (circles) as well as vertical (asterisks) cross sections of transient aberration distribution in a sample subjected to heating radiation.

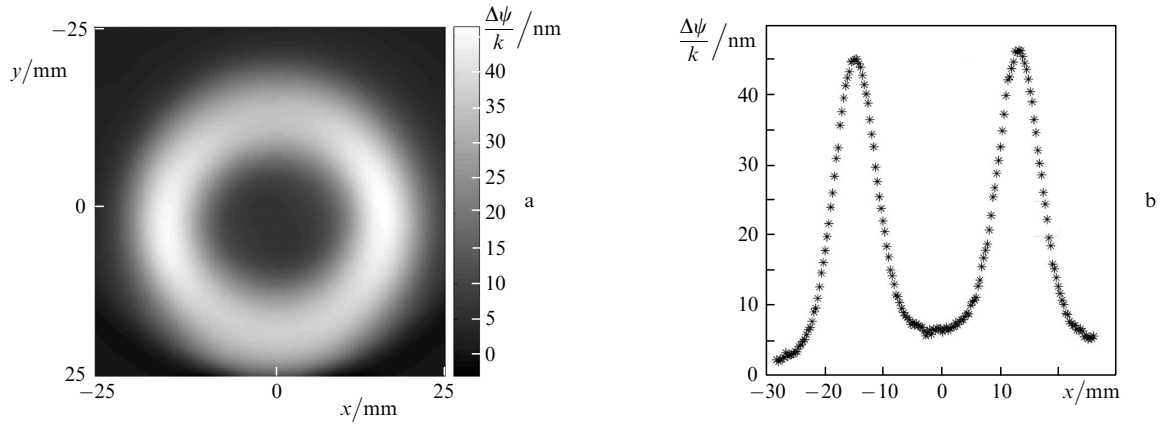

Figure 4. (a) Two-dimensional profile and (b) horizontal cross section of transient aberration distribution in a sample subjected to compensating radiation.

to the intensity profiles of heating and compensating radiation. This correspondence has been confirmed experimentally and can form the basis of an original technique for measuring radiation intensity profile in the far-IR range. Note that such a technique can be used for measurement of radiation profiles in not only infrared range, but microwave region also.

The system adjustment was carried out in two stages. Rough tuning was performed by using He–Ne laser (*10*), whose beam was made to coincide with the beam of CO_2 laser (*1*) . Final fine adjustment involved the combining of the centres of symmetries of distributions shown in Fig. 3 and 4 with the centre of the sample under study. This led to an axial symmetry of heat distribution and the results of the experiments can be expected to match the results of numerical calculations.

4. Discussion of results

Two series of experiments were carried out on the setup described above. In the first series, the parameters R and P of the compensating radiation were varied, while the parameters of the heating beam were left unchanged. This series of experiments was aimed at a comparison of the numerical and experimental results. In the second series, the numerically determined optimal parameters W_{opt}, R_{opt} and P_{opt} of the compensating radiation were realised for various powers of heating radiation.

Figures 5 and 6 show the results of the first series of experiments. The experimental data are shown by symbols, while solid curves show the theoretical wavefront distortions for the corresponding values of the compensating radiation parameters. One can see that there is a good agreement between the results of numerical simulation and the experimental data, and this raises hopes about the predicting ability of the programme code and the possibility of experimental realisation of the best compensation for a given heating beam by using the optimal parameters W_{opt}, R_{opt} and P_{opt} obtained from computations.

Figure 7 shows the distortions of the radiation wavefront measured for such optimal parameters. If the heating and compensating radiation powers are increased proportionally, the value of $\Delta\psi$ will increase in the same proportion because the problem is linear in the case of convective heat exchange. Consequently, the distribution of thermal dis-

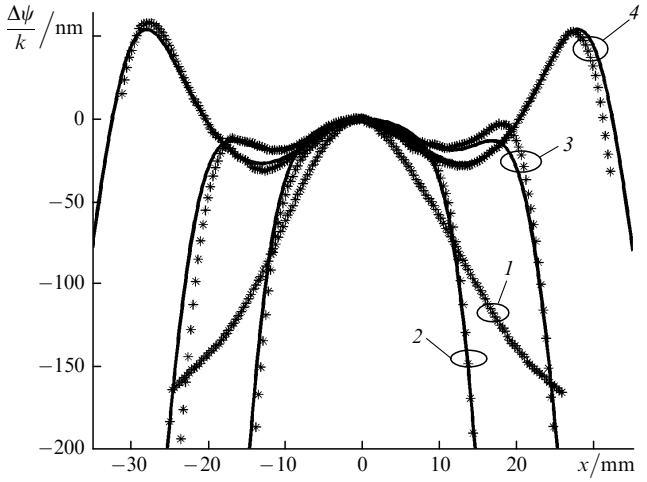

Figure 5. Phase distortions in a sample for compensating radiation parameter $R = \infty$ (*1*), 3.1 (*2*), 2.3 (*3*) and 1.5 cm (*4*) obtained as a result of numerical simulation (solid curves) as well as experimentally (symbols) for parameters $W = 18$ mm, $P = 4.3$ W, $P_0 = 250$ mW, and $w_0 = 10$ mm.

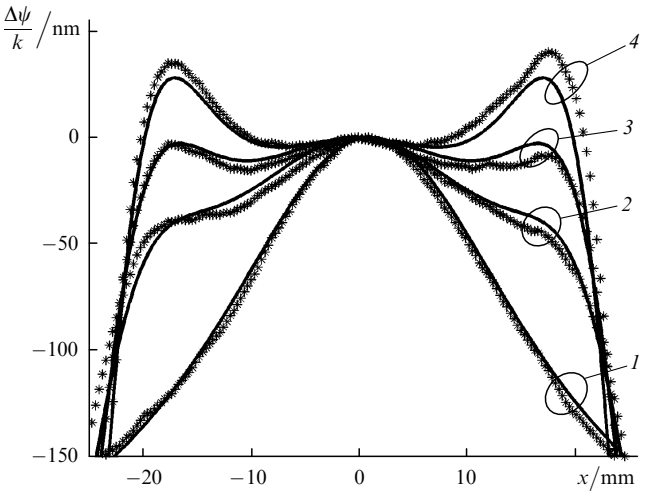

Figure 6. Phase distortions in a sample for compensating radiation parameter $P = 0$ (*1*), 2 (*2*), 3.5 (*3*) and 5.7 W (*4*) obtained as a result of numerical simulation (solid curves) as well as experimentally (symbols) for parameters $W = 18$ mm, $R = 22$ mm, $P_0 = 250$ mW, and $w_0 = 10$ mm.

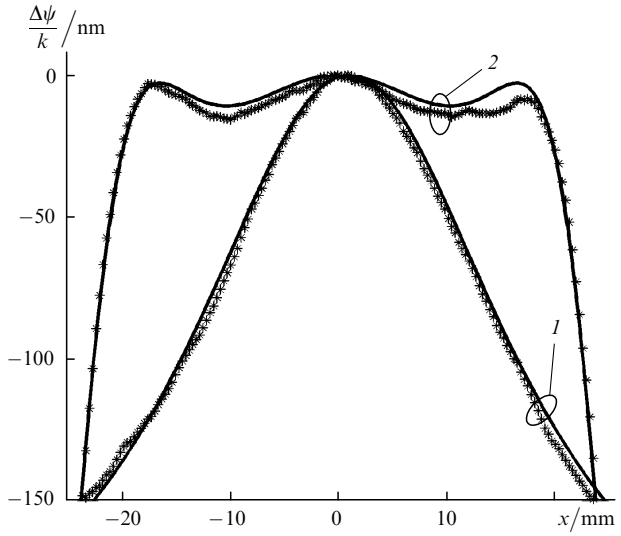

Figure 7. Phase distortions in a sample in the absence of compensating radiation ($\gamma = 0.116$) [curve (*1*)] and in the presence of compensating radiation for optimal values of parameters $W_{opt} = 18$ mm, $R_{opt} = 2.3$ cm, and $P_{opt} = 4.3$ W ($\gamma = 0.003$) [curve (*2*)]. Solid curves correspond to numerical simulation, while the experimental results (symbols) were obtained for parameters $P_0 = 250$ mW, and $w_0 = 10$ mm.

tortions in the presence of compensating radiation with optimal parameters W_{opt}, R_{opt} and P_{opt} differ only quantitatively for various values of the power P_0.

Compensation leading to a decrease in the parameter γ from 0.357 to 0.033, from 0.157 to 0.012 and from 0.116 to 0.003 was realised experimentally (Fig. 8). The squares in Fig. 8 correspond to the experimentally obtained phase distortions $\Delta\psi(x, y)$ caused by heating radiation only, while the circles correspond to distortions in the presence of compensating radiation. The integrand in formula (3) contains nonlinear functions for temperature-induced phase shift $\Delta\psi$, and hence the dependence of γ on the heating radiation power is nonlinear. Solid curves show the theoretical dependence of γ on P_0 for the remaining parameters (beam radii, radius of the compensating ring, ratio of heating and compensating radiation powers) corresponding to the experiment carried out for $P_0 = 500$ mW. The experimental points corresponding to $P_0 = 250$ and 300 mW coincide almost exactly with the curve obtained without compensation (squares) and are even slightly lower than the curve obtained with compensation (circles). Apparently, this is due to a certain dependence of the shape of the heating beam on the laser power.

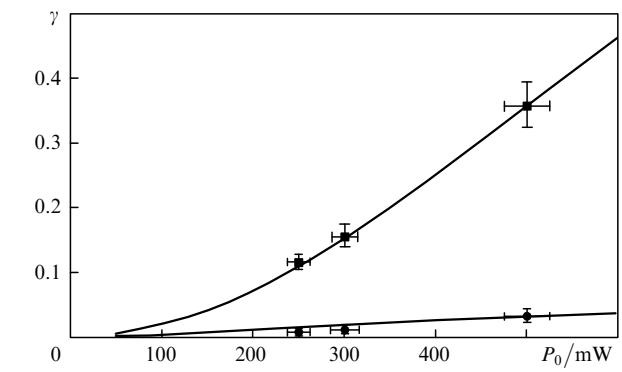

Figure 8. Theoretical (curves) and experimental (symbols) dependences of the parameter γ on the heating radiation power, obtained in the presence (●) and absence (■) of compensating radiation.

On the whole, Figs 5–8 reveal a good agreement of the results of numerical calculations with the experimental results, as well as a high efficiency of the compensation technique.

5. Conclusions

Thus, we have verified experimentally the method of active compensation for phase distortions in optical elements. For this purpose, we chose the simplest setup from the experimental point of view, in which ring-type heating was performed by a Gaussian CO_2 laser beam moving uniformly along a circle.

The programme code developed by us makes it possible to calculate the optimal parameters of compensating radiation, e.g., radius W_{opt} and power P_{opt} of the rotating beam, as well as the radius R_{opt} of its trajectory on the sample aperture. The parameters are assumed to be optimal if the power losses γ can be minimised in the fundamental mode of radiation. The programme allows us to calculate the distortion for an arbitrary (heating as well as compensating) heat source of cylindrical symmetry. The experiments revealed that the programme code has a predicting ability for forecasting thermal aberrations and their compensation.

A decrease in the parameter γ from 0.357 to 0.033, from 0.157 to 0.012 and from 0.116 to 0.003 was realised in three experiments for known numerical values of optimal parameters of the compensating radiation for distorting heat release power of 250, 300 and 500 mW respectively. Consequently, it can be stated that auxiliary heating with the help of extraneous laser radiation can be used effectively for compensating thermal phase distortions in optical elements.

The main advantages of the techniques proposed by us are contactless heating, simplicity of realisation, and the possibility of rapid rearrangement of the setup for compensation of distortions caused by laser beams of various diameters and intensities. However, it must be borne in mind while estimating the efficiency of this method that in the case of auxiliary heating, the compensation naturally entails an increase in the average temperature of the element and this may emerge as a serious drawback in some cases.

Note that the method described here can be improved considerably. For example, if the rotational velocity of the compensating radiation beam is modulated within each period, the regions in which the motion is slower will be heated more intensely. If the radius of the heating ring is varied rapidly by varying the angle between the normal to the mirror and the rotational axis, distributions with a more complex dependence on the radial coordinate will be realised.

Acknowledgements. This work was supported by the National Science Foundation (NSF) of the USA (Grant No. PHY-0457107).

References

1. Levine F. *IEEE J. Quantum Electron.*, **7** (4), 170 (1971).
2. Yang H., Liu J., Shen D., Tam S.-C., Lam Y.-L., Xie W., Kobayashi T. *Opt. Rev.*, **8** (3), 163 (2001).

3. Hua R., Wada S., Tashiro H. *Opt. Commun.*, **175** (4-6), 189 (2000).
4. Khazanov E.A. *Kvantovaya Electron.*, **30**, 147 (2000) [*Quantum Electron.*, **30**, 147 (2000)].
5. Bespalov V.I., Pasmanik G.A. *Nelineinaya optika i adaptivnye lazernye sistemy* (Nonlinear Optics and Adaptive Laser Systems) (Moscow: Nauka, 1985).
6. Kurczynski P., Dyson H.M., Sadoulet B., Bower J.E., Lai W.Y.-C., Vansfield W.M., Taylor J.A. *Appl. Opt.*, **43** (18), 3573 (2004).
7. Webb R.H., Albanese M.J., Zhou Y., Bifano T., Burns S. *Appl. Opt.*, **43** (28), 5330 (2004).
8. Troitskii I.N., Safronov A.N. *Adaptivnaya optika* (Adaptive Optics) (Moscow: Znanie, 1989).
9. Weber R., Graf T., Weber H.P. *IEEE J. Quantum Electron.*, **36** (6), 757 (2000).
10. Roth M.S., Wyss E.W., Graf T., Weber H.P. *IEEE J. Quantum Electron.*, **40** (12), 1700 (2004).
11. Mueller G., Amin R.S., Guagliardo D., McFeron D., Lundock R., Reitze D.H., Tanner D.B. *Classical and Quantum Gravity*, **19**, 1793 (2002).
12. Khazanov E.A., Andreev N.F., Mal'shakov A.N., Palashov O.V., Poteomkin A.K., Sergeev A.M., Shaykin A.A., Zelenogorsky V.V., Ivanov I., Amin R.S., Mueller G., Tanner D.B., Reitze D.H. *IEEE J. Quantum Electron.*, **40** (10), 1500 (2004).
13. Khazanov E.A., Zelenogorsky V.V., Shaykin A.A., Kamenetsky E.E., Palashov O.V. *Proc. Int. Symp. on Topical Problems of Nonlinear Wave Physics* (St.Petersburg – N.Novgorod, 2005) pp 137, 138.
14. Lawrence R., Zucker M., Fritschel P., Marfuta P., Shoemaker D. *Classical and Quantum Gravity*, **19**, 1803 (2002).
15. Lawrence R., Ottaway D., Zucker M., Fritschel P. *Opt. Lett.*, **29** (22), 2635 (2004).
16. Abramovici A., Althouse W.E., Drever R.W.P., Gursel Y., Kawamura S., Raab F.J., Shoemaker D., Sievers L., Spero R.E., Thorne K.S., Vogt R.E., Weiss R., Whitcomb S.E., Zucker M.E. *Science*, **256**, 325 (1992).
17. Mezenov A.V., Soms L.N., Stepanov A.I. T*ermooptika tverdotel'nykh lazerov* (Thermooptics of Solid-State Lasers) (Leningrad: Mashinostroenie, 1986).
18. Landau L.D., Lifshits E.M. *Fluid Mechanics* (Oxford: Pergamon Press, 1987; Moscow: Nauka, 1988).
19. Samarskii A.A., Nikolaev E.S. *Metody resheniya setochnykh uravnenii* (Methods of Solving Network Equations) (Moscow: Nauka, 1978) .
20. Landau L.D., Lifshits E.M. *Course of Theoretical Physics, Vol. 7 (Theory of Elasticity)* (Oxford: Pergamon Press, 1970; Moscow: Nauka, 2004).
21. Amosov A.A., Dubinskii Yu.A., Kopchenova N.V. *Vychislitel'nye methody dlya inzhenerov* (Computational Methods for Engineers) (Moscow: Vysshaya shkola, 1994).
22. Kozhevatov I.E., Rudenchik E.A., Cheragin N.P., Kulikova E.H. *Radiophys. Quantum Electron.*, **44** (7), 575 (2001).
23. Sommarggren G.E. *Laser Focus World*, **32** (8), 61 (1996).
24. Zelenogorsky V.V., Solovyov A.A., Kozhevatov I.E., Kamenetsky E.E., Rudenchik E.A., Palashov O.V., Silin D.E., Khazanov E.A. *Appl. Opt.*, **45**, 17 (2006).